Molecular Crystals and Liquid Crystals

ISSN: 1542-1406 (Print) 1563-5287 (Online) Journal homepage: http://www.tandfonline.com/loi/gmcl20

Comparison of mesomorphic properties exhibited by linear hydrogen bonded thermotropic liquid crystals

P. Rohini, N. Pongali Sathya Prabu & M. L. N. Madhu Mohan

To cite this article: P. Rohini, N. Pongali Sathya Prabu & M. L. N. Madhu Mohan (2016) Comparison of mesomorphic properties exhibited by linear hydrogen bonded thermotropic liquid crystals, Molecular Crystals and Liquid Crystals, 631:1, 74-91, DOI: 10.1080/15421406.2016.1149022

To link to this article: http://dx.doi.org/10.1080/15421406.2016.1149022

MOLECULAR CRYSTALS AND LIQUID CRYSTALS
2016, VOL. 631, 74–91
http://dx.doi.org/10.1080/15421406.2016.1149022

Taylor & Francis
Taylor & Francis Group

Comparison of mesomorphic properties exhibited by linear hydrogen bonded thermotropic liquid crystals

P. Rohini, N. Pongali Sathya Prabu, and M. L. N. Madhu Mohan

Liquid Crystal Research Laboratory (LCRL), Bannari Amman Institute of Technology, Sathyamangalam, India

ABSTRACT

Two linear hydrogen-bonded liquid crystal homologous series have been isolated in the present investigation and compared. Palmitic acid is chemically bonded with alkyloxy benzoic acids, and alkyl benzoic acids to yield 15 mesogenic complexes. The formation of inter molecular hydrogen bonding is confirmed by Fourier transform infrared spectroscopy (FTIR). Phase polymorphism exhibited by the two linear homologous series is evinced by various textural observations made through polarizing optical microscopic (POM) studies. Differential scanning calorimetry (DSC) studies revealed the transition temperatures and the corresponding enthalpy values exhibited by the individual phases. Phase diagrams has been constructed through POM and DSC data. Thermal equilibrium, thermal stability factor, and order of phase transition data are obtained from DSC study. Influence of oxygen atom attached/detached to the rigid chemical moiety toward the properties of the homologous series is discussed. Light filtering action of the nematogens at different temperatures is also conferred.

KEYWORDS

Linear hydrogen-bonded liquid crystals; light filtering action; odd-even effect; order of transition; thermal equilibrium

Introduction

Liquid crystal display (LCD) device technology finds a prosperous path in the recent epoch due to its impact over electronic devices [1]. LCD thrives over when compared to the other display technologies due to its environmental mode of fitting [2]. Chemical ingredients utilized in LCD panel plays a key role in determining the quality and efficacy of the display devices [3, 4]. Hydrogen-bonded liquid crystals (HBLCs) a broad area of research under thermotropic liquid crystals proves itself to be one of the best chemical component for display devices due to the ease of formation of mesogenic materials or stabilize the liquid crystallinity when the length of the rigid rod chemical moiety is being increased [5,6]. Abundant existence of acceptor and donor functional groups, self-assembly nature existence, and the applicational aspects are the reasons, which made the researchers to investigate HBLC extensively [7]. Carboxylic acids are the first compounds found to exhibit mesogenic nature due to the formation of hydrogen bonding. Trans–p–methoxy cinnamic acids [8], trans-p-ethoxy cinnamic acids [9], and p-n-alkyloxy benzoic acids (nBAO) [10] are some of the carboxylic acids, which form liquid crystalline property.

CONTACT M. L. N. Madhu Mohan mln.madhu@gmail.com Liquid Crystal Research Laboratory (LCRL), Bannari Amman Institute of Technology, Sathyamangalam, India
Color versions of one or more of the figures in the article can be found online at www.tandfonline.com/gmcl.

Preparation of HBLC materials for applicational purposes is a challenging and interesting task. Alkyl/alkyloxy benzoic acids, which are mesogenic in nature [10], form complimentary hydrogen bonds with any aliphatic acids giving rise to HBLC. It is reported that when any mesogenic/non mesogenic moiety is interacted with alkyloxy benzoic acids, HBLC are formed with single [11–15], double [16–20], and multiple hydrogen bonds [21–25]. Mesogenic nature depends on the products nature. These hydrogen-bonded materials can be used for applications only if it possesses a wide thermal mesophase. The design of the molecular structure helps in a proper molecular alignment of the phase, which plays a pivotal role in ascertaining the extent of utility of the mesogen. With our previous experience in synthesis and characterizing [11–20] various types of liquid crystals two novel series of hydrogen-bonded mesogens are synthesized.

The central theme of the aimed research work involves in design, synthesis, and characterization and comparison of mesomorphic properties of 15 mesogenic complexes formed between palmitic acid (PA), various nBAO, where *n* varies from 5 to 12 and various alkyl benzoic acids (nBA), where *n* varies from 2 to 8. The mesogenic nature exhibited by the homologues due to the presence/absence of an electronegative atom to the rigid part and other relevant properties are elaborated in the present investigation.

Experimental

Optical textural observations of the formed complexes are made with a Nikon polarizing microscope equipped with Nikon digital CCD camera system with 5mega pixels and 2560*1920 pixel resolutions. The liquid crystalline textures are processed, analyzed and stored with the aid of Nikon Imaging Software system. The temperature control of the liquid crystal cell is equipped with Instec HCS402-STC 200 temperature controller (Instec, USA) to a temperature resolution of $\pm$ 0.1°C. This unit is interfaced to computer by IEEE–STC 200 to control and monitor the temperature. The transition temperatures and corresponding enthalpy values are obtained by differential scanning calorimetry (DSC) (Shimadzu DSC-60, Japan). Fourier transform infrared (FTIR) spectra is recorded (ABB FTIR MB3000) and analyzed with the MB3000 software. PA, nBAO, and nBA are supplied by Sigma Aldrich (Germany) and all the solvents used are high-performance liquid chromatography grade.

Synthesis of HBLC

Intermolecular hydrogen bonded mesogens are synthesized by the addition of one mole of (PA) with one mole of nBAO, where *n* represents pentyloxy to dodecyloxy benzoic acid) in N, N-dimethyl formamide (DMF). The same mole ratio is followed to prepare PA + nBA homologous series (where *n* represents ethyl to octyl benzoic acid). Further, they are subjected to constant stirring for 12 hr at ambient temperature of 30°C till a white precipitate in a dense solution is formed. Schematic representation of PA + nBAO and PA + nBA homologous series formation is depicted as scheme 1 and scheme 2, respectively. Atomic arrangement of the lower alkyloxy carbon number (5BAO) and higher alkyloxy carbon number (12BAO) with PA are shown as Figs. 1a and 1b. Similarly, the atomic arrangement of lower alkyl carbon number (2BA) and higher alkyl carbon number (8BA) along with PA are shown as Figs. 1c and 1d, respectively.

Results and discussion

Fifteen hydrogen-bonded complexes isolated under the present investigation are of white crystalline solids and are stable at room temperature (30°C). They are insoluble in water

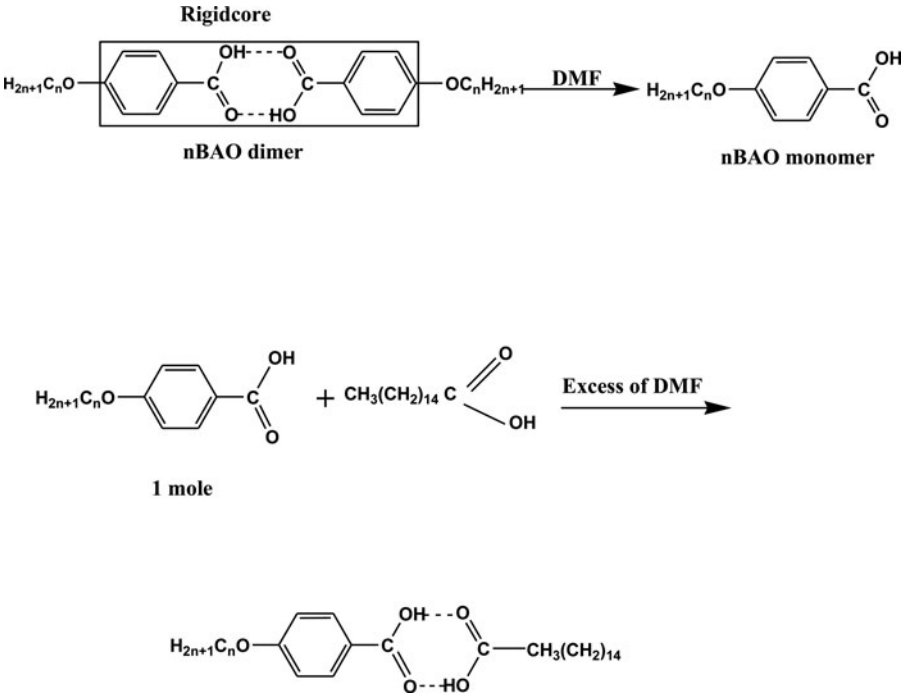

Scheme 1. Schematic representation of PA + nBAO homologous formation.

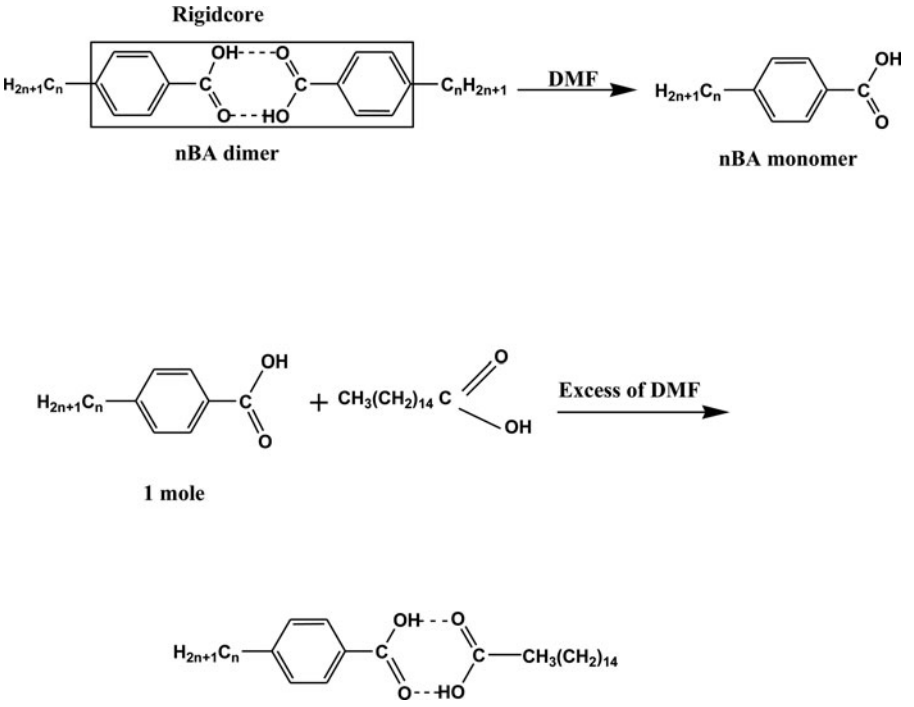

Scheme 2. Schematic representation of PA + nBA homologous formation.

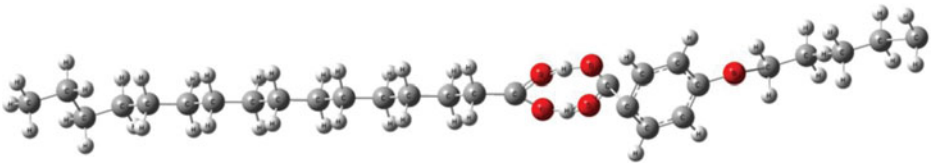

Figure 1a. Atomic structure of PA + 5BAO complex.

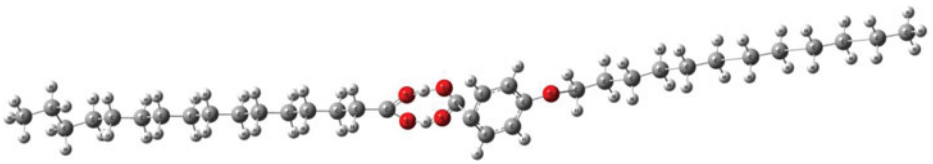

Figure 1b. Atomic structure of PA + 12BAO complex.

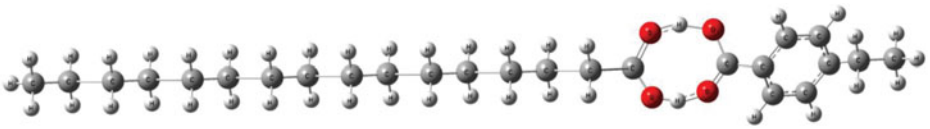

Figure 1c. Atomic structure of PA + 2BA complex.

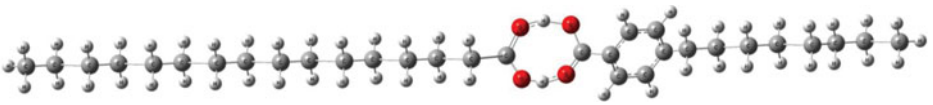

Figure 1d. Atomic structure of PA + 8BA complex.

and sparingly soluble in common organic solvents such as methanol, ethanol, benzene and dichloromethane. However, they show a high degree of solubility in coordinating solvents like dimethyl sulfoxide, DMF, and pyridine. All these mesogens melt at specific temperatures ~ 54.7°C (Tables 1 and 2). They show the similar results when subjected to repeated thermal scans performed during polarizing optical microscopic (POM) and DSC studies indicating the thermal and chemical stability of the complexes formed.

Phase identification

The observed phase variance, transition temperatures and corresponding enthalpy values obtained by DSC in cooling and heating cycles for the PA + nBAO and PA + nBA homologues are presented in Tables 1 and 2.

PA + nBAO homologous series

The mesogens of PA + nBAO homologous series are found to exhibit characteristic textures [26], viz., nematic (threaded texture, plate 1) and smectic G (multi colored smooth mosaic like texture, plate 2), respectively. The phase sequence of PA + nBAO series obtained by POM and

Table 1. Thermal parameters obtained for PA + nBAO series.

Complex	Phase variance	DSC	Crystal to melt	*N*	G	Crystal
PA + 5BAO	G	H	62.1 (92.94)		100.9 (14.22)	
		C			83.7 (16.12)	55.8 (93.52)
		POM			84.1	56.2
PA + 6BAO	G	H	60.5 (111.89)		#	
		C			69.7 (9.16)	51.9 (107.56)
		POM			70.2	52.4
PA + 7BAO	G	H	61.4			
(79.52)		#				
		C			54.1 (1.98)	50.0 (90.78)
		POM			54.6	50.8
PA + 8BAO	G	H	60.9 (78.20)		75.7 (8.30)	
		C			73.4 (6.59)	51.0 (83.48)
		POM			73.9	51.6
PA + 9BAO	NG	H	62.3 (79.48)		#	
		C		63.5 (4.86)	56.5 (Merged with K)	54.5 (111.27)
		POM		64.3	57.2	55.1
PA + 10BAO	NG	H	60.5 (75.98)		82.8 (12.45)	
		C		93.5 (5.03)	74.4 (7.44)	51.4 (70.74)
		POM		94.3	74.9	51.6
PA + 11BAO	NG	H	61.3 (49.45)	91.9 (30.49)	#	
		C		83.6 (3.29)	66.4 (19.45)	53.2 (54.75)
		POM		84.4	67.1	53.5
PA + 12BAO	NG	H	62.0 (64.52)	90.5 (37.59)	#	
		C		86.1 (3.49)	65.6 (18.86)	54.9 (63.84)
		POM		86.9	66.1	55.2

H–Heating run, C–Cooling run, #-monotropic transition.
Enthalpy in parenthesis given in J/g, Temperature in °C.

Table 2. Thermal parameters obtained for PA + nBA series.

Complex	Phase variance	DSC	Crystal to melt	G	Crystal
PA + 2BA	G	H	56.0 (87.82)	#	
		C		52.9 (0.67)	47.9 (79.08)
		POM		53.3	48.1
PA + 3BA	G	H	60 (91.37)	#	
		C		60.3 (1.78)	53.3 (91.48)
		POM			
PA + 4BA	G	H	54.9 (104.41)	#	
		C		51.9 (0.01)	45.1 (104.35)
		POM		52.2	45.5
PA + 5BA	G	H	54.7 (107.96)	#	
		C		48.0 (0.09)	44.4 (109.58)
		POM		48.5	44.8
PA + 6BA	G	H	55.6 (110.88)	#	
		C		49.3 (1.84)	42.0 (105.40)
		POM		49.7	42.2
PA + 7BA	G	H	57.5 (98.61)	#	
		C		54.9 (6.55)	48.1 (95.91)
		POM		55.2	48.3
PA + 8BA	G	H	57.5 (70.88)	#	
		C		49.7 (1.64)	47.3 (64.34)
		POM		50.1	47.5

H–Heating run, C–Cooling run, #-monotropic transition.
Enthalpy in parenthesis given in J/g, Temperature in °C.

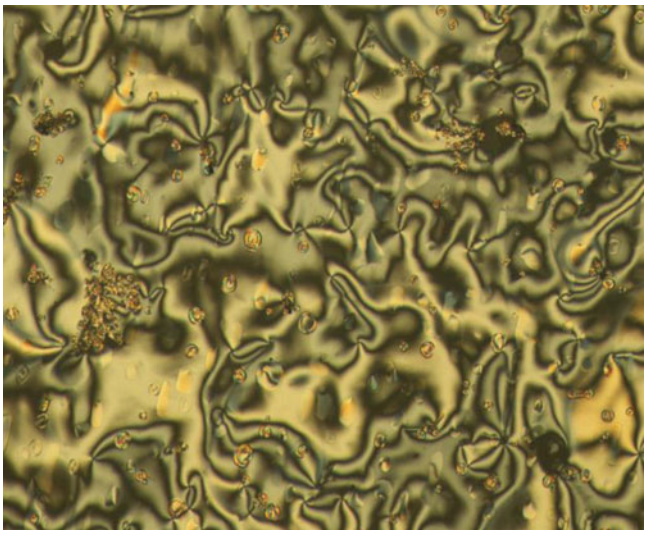

Plate 1. Thread like texture of nematic phase observed in PA + 11BAO complex at 80.5°C.

DSC studies can be represented as below:

$$\begin{aligned}
Isotropic &\rightleftharpoons Sm\,G \rightleftharpoons Crystal && (PA+5BAO,\ PA+8BAO)\\
Isotropic &\rightarrow Sm\,G \rightleftharpoons Crystal && (PA+6BAO,\ PA+7BAO)\\
Isotropic &\rightarrow \mathrm{N} \rightarrow Sm\,G \rightleftharpoons Crystal && (PA+9BAO)\\
Isotropic &\rightarrow N \rightleftharpoons Sm\,G \rightleftharpoons Crystal && (PA+10BAO)\\
Isotropic &\rightleftharpoons N \rightarrow Sm\,G \rightleftharpoons Crystal && (PA+11BAO,\ PA+12BAO)
\end{aligned}$$

Single and double arrow indicates monotropic and enantiotropic transitions, respectively.

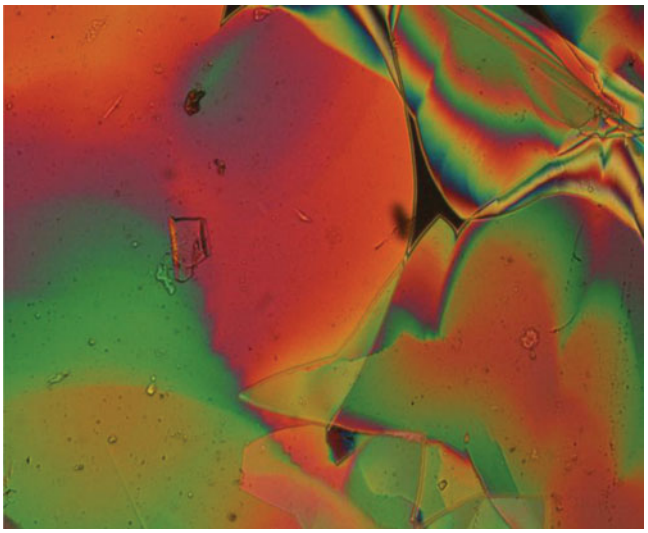

Plate 2. Smooth multicolored mosaic like texture of smectic G phase observed in PA + 5BAO complex at 70.5°C.

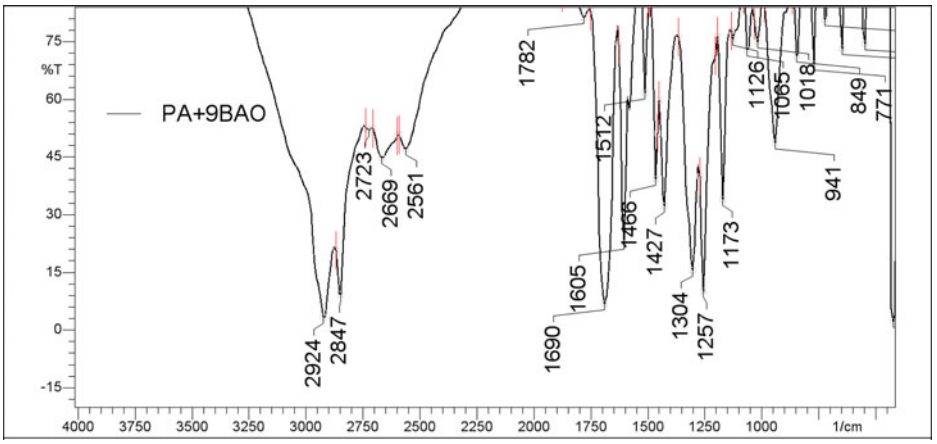

Figure 2a. FTIR spectrum of PA + 9BAO complex.

PA + nBA homologous series

Mesogenic complexes of PA + nBA homologous series are found to exhibit mono phase variance, viz., high-ordered smectic G phase. Absence of electronegative oxygen atom in the terminal group has quenched the isotropic transition temperature to a greater extent of PA + nBA series when compared with PA + nBAO series. Moreover, smectic G transition temperature is also drastically reduced (Table 2). Absence of the oxygen atom to the terminal chemical moiety is confined be the possible reason which have stopped triggering the inducement of any mesogenic phase except the higher ordered smectic G phase. The phase sequence of PA + nBA series obtained by POM and DSC studies can be represented as below:

$$\text{Isotropic} \rightarrow \text{Sm G} \rightleftharpoons \text{Crystal} \qquad (\text{PA} + \text{nBA}, \text{n} = 2 \text{ to } 8)$$

Infrared spectroscopy

IR spectra for all the fifteen homologues of PA + nBAO and PA + nBA series have been recorded in the solid state (KBr) at room temperature. As a representative case, FTIR spectrum of PA + 9BAO complex is shown in Fig. 2a for PA + nBAO series and the spectra

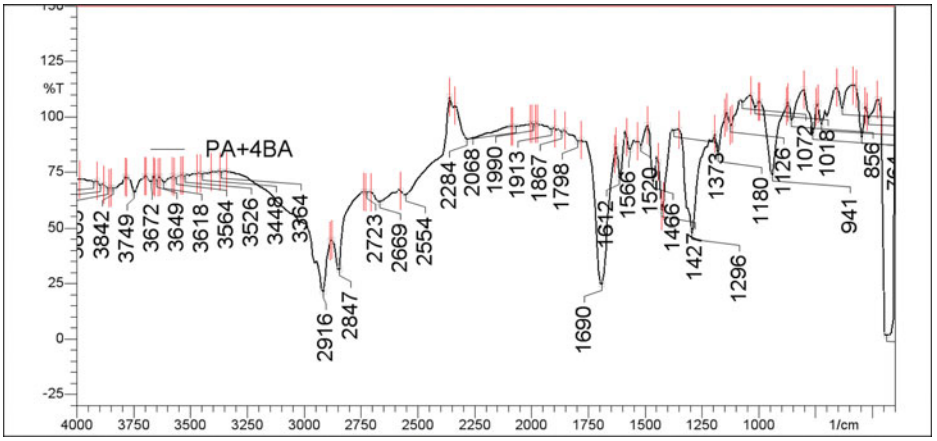

Figure 2b. FTIR spectrum of PA + 4BA complex.

Table 3. FTIR data obtained for PA + nBAO and PA + nBA series along with their precursors.

	Complex		Corresponding Precursor			Complex		Corresponding Precursor	
Complex	OH	COOH	OH	COOH	Complex	OH	COOH	OH	COOH
PA + 12BAO	2924	1690	2924	1674	PA + 8BA	2924	1690	2932	1682
PA + 11BAO	2916	1690	2924	1674	PA + 7BA	2924	1697	2924	1697
PA + 10BAO	2924	1690	2924	1674	PA + 6BA	2924	1690	2924	1682
PA + 9BAO	2924	1690	2924	1674	PA + 5BA	2916	1690	2955	1690
PA + 8BAO	2924	1690	2924	1674	PA + 4BA	2916	1690	2955	1690
PA + 7BAO	2924	1690	2924	1690	PA + 3BA	2916	1690	2962	1682
PA + 6BAO	2916	1697	2932	1682	PA + 2BA	2916	1697	2924	1674
PA + 5BAO	2916	1682	2939	1666					

corresponding to PA + 4BA for PA + nBA series is shown as Fig. 2b and is discussed elaborately. It is reported [27, 28] that in the nBAO, carboxylic acid exists in monomeric form and the stretching vibration of C = O is observed at 1782 cm^{-1}. Further, it is known [28] that when a hydrogen bond is formed between carboxylic acids it results in lowering of the carbonyl frequency, which has been detected in the present hydrogen-bonded complexes also. A noteworthy feature in the spectrum of the PA + 9BAO complex (Fig. 2a) is the appearance of sharp peak at 1690 cm^{-1}, which clearly suggests the dimer formation in particular the carbonyl group vibration. [29–31]. The same vibrational peak corresponding to dimer formation is observed for the PA + 4BA complex also (Fig. 2b). A carboxylic acid existing in monomeric form in dilute solution absorbs at about 1782 cm^{-1} because of the electron withdrawing effect. However, acids in concentration solution or in solid state tend to dimerize through hydrogen bonding. It is reported [28] that this dimerization weakens the C=O bond and lowers the stretching force constant K, resulting in a lowering of the carbonyl frequency of saturated acids to ~1700 cm^{-1}.This result concurs with the reported data of Kato et al [31]. Moreover, a sharp intense peak obtained at 2924 cm^{-1} in PA + 9BAO complex and at 2916 cm^{-1} in PA + 4BA complex is assigned to the (O-H) bond formation, confirming the intermolecular hydrogen bond existence between the synthesized complexes. Hence, in the present complexes the formation of hydrogen bonding is established by FTIR. A similar trend of result is followed in all the synthesized hydrogen-bonded complexes of PA + nBAO and PA + nBA series. Table 3 represents the peak assignment corresponding to the OH and COOH vibrations of the synthesized PA + nBAO and PA + nBA complexes along with their respective precursors.

DSC studies

DSC thermograms are obtained in heating and cooling cycle. The sample in the crimped aluminum cell is heated with a scan rate of 10°C/min and held at its isotropic temperature for 2 min so as to attain thermal stability. The cooling run is performed with a programmed scan rate of 10°C/min. The respective equilibrium transition temperatures and corresponding enthalpy values of the various homologues are listed in Tables 1 and 2. These DSC results concur with the POM data.

DSC study of PA + 12BAO

As a representative case, the DSC thermogram of PA + 12BAO complex is discussed elaborately which is shown as Fig. 3a. From Table 1 and Fig. 3a, it can be inferred that the DSC cooling run exhibits three exothermic peaks at 86.1, 65.6, and 54.9°C with enthalpy values

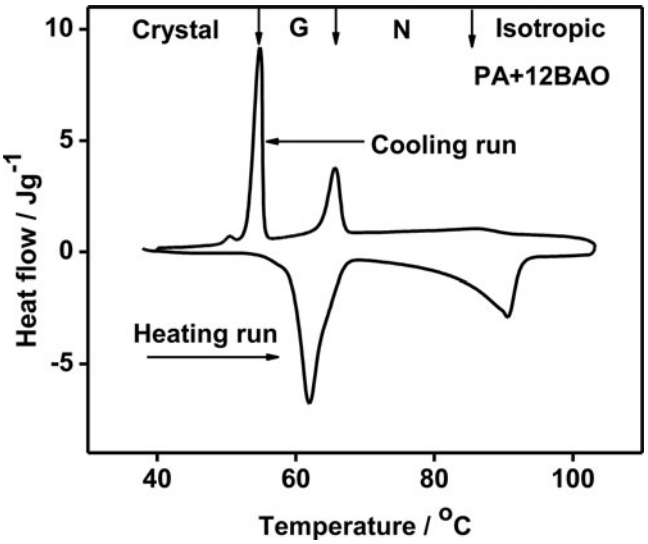

Figure 3a. DSC thermogram of PA + 12BAO complex.

of 3.49, 18.86, and 63.84 Jg^{-1}, respectively. The three distinct peaks observed in the cooling run corresponds to isotropic to nematic, nematic to smectic G, and smectic G to crystal phase transition, respectively. In the heating run of DSC, two distinct peaks are obtained for the same complex at temperatures 62.0 and 90.5°C possessing an enthalpy value of 64.52 and 37.59 Jg^{-1}, respectively. These peaks correspond to crystal to melt and smectic G to nematic phase transition. Melt to smectic G transition is observed to be monotropic transition whereas the remaining is said to possess enantiotropic transitions. The DSC exothermic curves of all the PA + nBAO complexes have been depicted in Fig. 3b along with their phase variance.

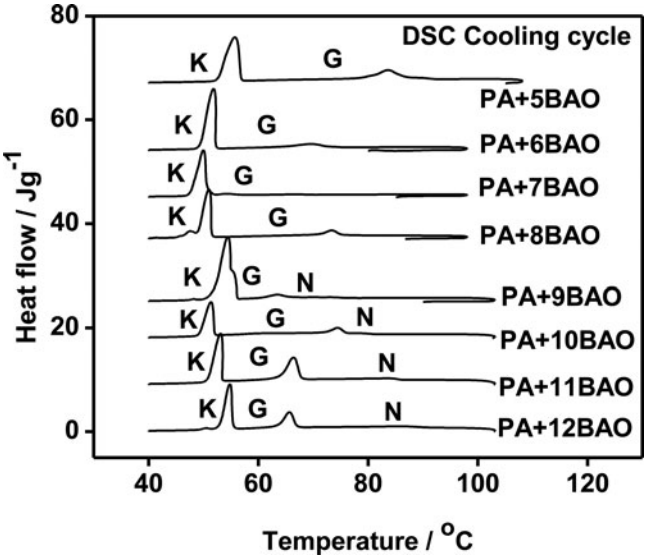

Figure 3b. Exothermic peaks obtained for PA + nBAO homologous series.

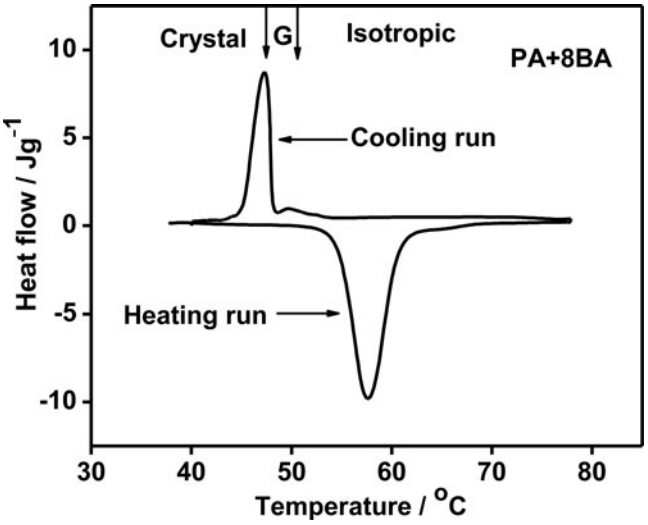

Figure 4a. DSC thermogram of PA + 8BA complex.

DSC study of PA + 8BA

DSC is performed to all the seven complexes of PA + nBA series also. As a representative case, the DSC thermogram of PA + 8BA complex is discussed elaborately which is shown as Fig. 4a. From Table 2 and Fig. 4a, it can be inferred that the DSC cooling run exhibits two exothermic peaks at 49.7 and 47.3°C with enthalpy values of 1.64 and 64.34 Jg^{-1}, respectively. The two distinct peaks observed in the cooling run corresponds to isotropic to smectic G and smectic G to crystal phase transition, respectively. In the heating run of DSC, a distinct peak is obtained for the same complex at the temperature 57.5°C with an enthalpy value of 70.88 Jg^{-1} indicating crystal to melt transition. Melt to smectic G transition is observed to be monotropic transition. The DSC exothermic curves of all the PA + nBA complexes have been depicted in Fig. 4b along with their phase variance.

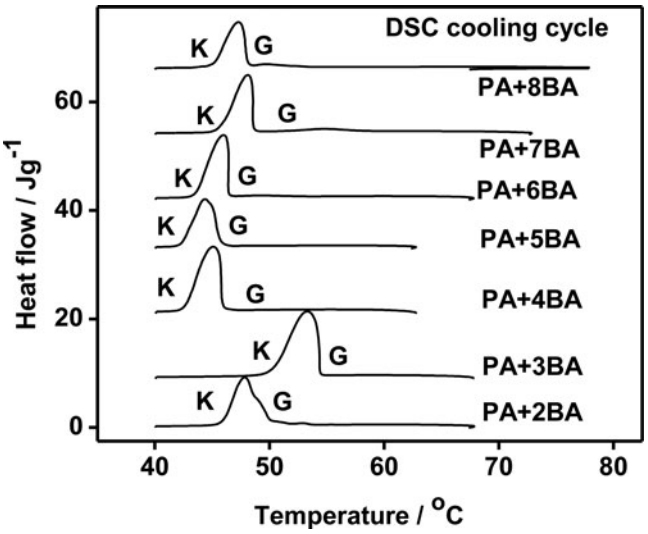

Figure 4b. Exothermic peaks obtained for PA + nBA homologous series.

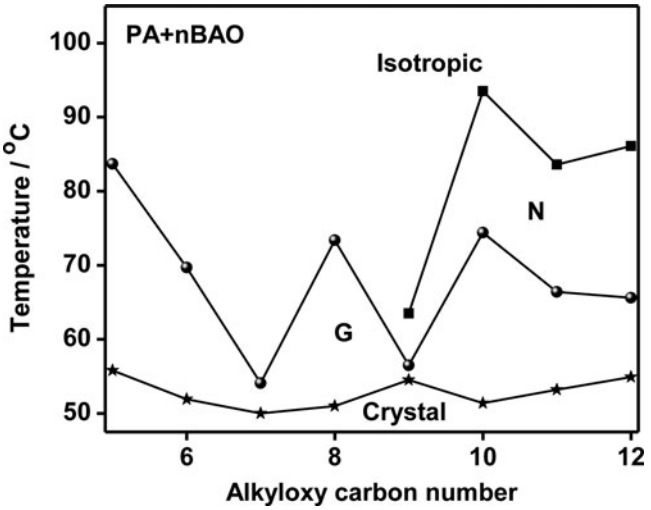

Figure 5a. Phase diagram of PA + nBAO series.

Phase diagrams

Phase diagram of PA + nBAO

Figure 5a illustrates the phase diagram of PA + nBAO homologous series. Following conclusions can be made from the phase diagram.

(i) Phase diagram of the present PA + nBAO homologous series consists of two phases, viz., nematic and Smectic G.
(ii) High-ordered smectic G phase is observed in the entire complexes prepared, while nematic phase is observed from PA + 9BAO and extends till PA + 12BAO.
(iii) Quenching in thermal span of smectic G is noticed by the inducement of nematic phase.
(iv) l/d ratio of the complexes are responsible for the inducement of nematic phase in the higher homologues.
(v) Presence of oxygen atom increases the alkyl chain length thereby the flexibility of the chemical chain thus favoring the phase polymorphism of the present PA + nBAO series.

For quantitative analysis of the homologous series, the phase diagram of PA + nBAO series is further examined in terms of percentage of the area occupied by individual mesophase. The percentage of the area occupied by each of the phase exhibited is mathematically calculated by trapezoidal rule. The percentage of the area occupied by the two phases namely nematic and smectic G exhibited in the present series 32.14% and 68.60%, respectively. Thus two third of the entire thermal span of the mesogenic range is occupied by smectic G phase.

Phase diagram of PA + nBA

Figure 5b illustrates the phase diagram of PA + nBA homologous series. Following conclusions can be made from the phase diagram.

(i) All the complexes exhibit mono phase variance, viz., high-ordered smectic G phase.
(ii) Isotropic transition temperature and smectic G phase transition temperatures are drastically reduced.
(iii) Absence of electronegative oxygen atom at the terminal group and therefore decrease in chemical chain length have suppressed the flexibility of the alkyl chain which in turn alters the mesogenic nature of the complexes.

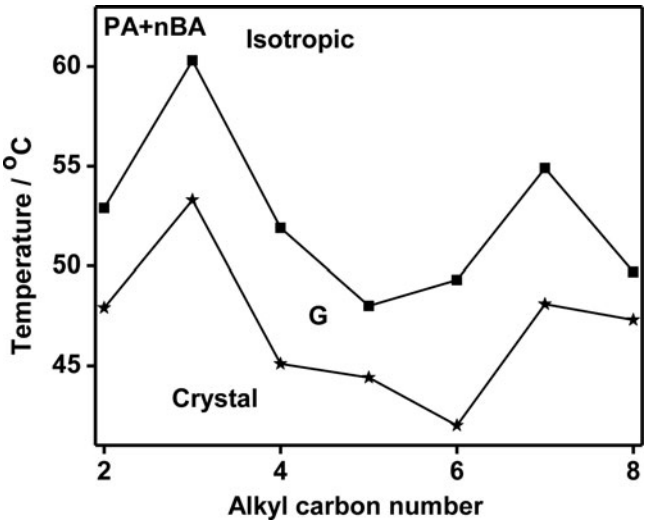

Figure 5b. Phase diagram of PA + nBA series.

Odd-even effect across isotropic to smectic G of PA + nBAO homologous series

The origin of the odd-even effect can be understood from the consideration of the chemical structure of the mesogen. In the even numbers of the series, the disposition of the end group is such as to enhance the molecular anisotropy and hence molecular order, whereas in the odd number it has the opposite effect. As the chain length increases, their flexibility increases and the odd-even effect becomes less pronounced. The results of the odd-even effect observed in the present series are in accordance with the quantitative calculations proposed [32–36].

It may be noted that the present intermolecular hydrogen-bonded liquid crystalline complexes are composed of a rigid aromatic ring and a flexible hydrogen bonding part. The rigid core length varies with increment in the nBAO carbon chain. The liquid crystalline phase polymorphism (Table 1) and the associated enthalpy values with increment of alkyloxy carbon chain length are thus attributed to this part of the chemical structure. Moreover, the length (l) of the total HBLC varies with the alkyl carbon chain length, while the width (d) remains constant. Thus, the altering of l/d ratio triggers the phase variance in the homologous series in turn influences the phase transition temperatures and the corresponding enthalpy values. Hence, the rigid cores and l/d ratio plays a vital role in establishing the pronounced odd-even effect as evinced in the present homologous series.

In the present homologous series, odd-even effect is noticed across isotropic to nematic both in transition temperatures and corresponding enthalpy values. Plots are constructed with the transition temperatures of isotropic to nematic (Fig. 5a) and their corresponding enthalpy values along *y*-axis (Fig. 5c) and the carbon chain length along *x*-axis. From these figures, it can be observed that the magnitudes of the transition temperatures corresponding to the even homologous exhibit one type of behavior, while their odd counter parts show a different pattern. Similar trend of results are obtained in the corresponding enthalpy values also. In the literature, such behavior has been reported [33] and is referred as odd-even effect. Presence of oxygen atom favors the length of the chain (PA + nBAO), and thus favors the existence of odd-even effect. Absence of oxygen atom to the terminal group alters the length of the chain (l) to a greater extent and hence odd-even effect in PA + nBA homologous series is suppressed.

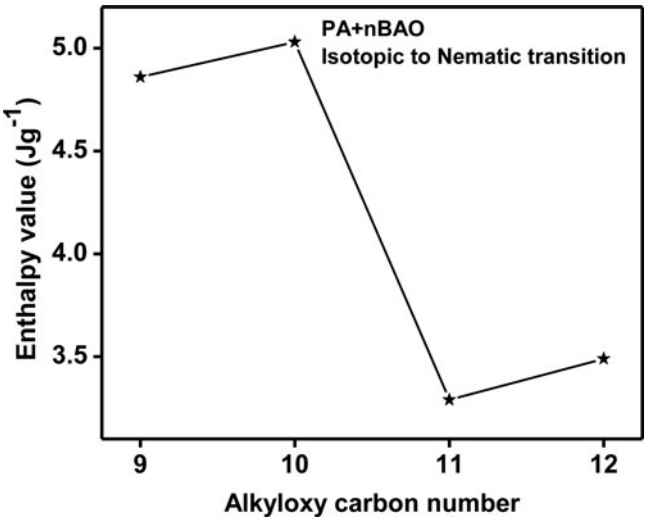

Figure 5c. Odd-Even effect observed across enthalpy value for isotropic-nematic phase transition temperature for PA + nBAO complexes.

Thermal equilibrium analysis

Thermal law of equilibrium is verified in the DSC thermal analysis cycles, viz., total enthalpy values evolved out of different phases observed in the heating cycle is compared with the enthalpy values obtained for the same phases in the cooling cycle for all the 15 complexes synthesized. In practical considerations, the summation of the enthalpy values possessed by the different phases in the heating cycle (endothermic reaction) will be slightly varied with the enthalpy value possessed by the same complex in the cooling cycle (exothermic reaction) as depicted in Table 4. Thus, the amount of heat evolved is equal to the heat absorbed in the given series. This thermal equilibrium condition prevails when all the transitions are enantiotropic. However, the deviation from the magnitudes in heating to cooling cycles may be attributed to the monotropic transitions present in the system.

Thermal stability of smectic G

Phase stability [37, 38] is one of the important parameters that govern the utility of the mesogen. In the present case, phase stability of smectic G is discussed. The term phase stability can be attributed to isotropic to smectic G transition temperature as well to the temperature range of smectic G phase. It is reasonable to consider both the above factors and define a parameter

Table 4. Thermal equilibrium exhibited by the individual PA + nBAO and PA + nBA complexes.

COMPLEX	HEATING RUN	COOLING RUN	COMPLEX	HEATING RUN	COOLING RUN
PA + 5BAO	107.16	109.64	PA + 2BA	87.82	79.75
PA + 6BAO	111.89	116.72	PA + 3BA	91.37	93.26
PA + 7BAO	94.86	92.76	PA + 4BA	104.41	104.36
PA + 8BAO	86.5	90.07	PA + 5BA	107.96	109.67
PA + 9BAO	113.05	116.13	PA + 6BA	110.88	107.24
PA + 10BAO	88.43	83.21	PA + 7BA	98.61	102.46
PA + 11BAO	79.94	77.49	PA + 8BA	70.88	65.98
PA + 12BAO	86.51	86.92			

J/g is the unit of heat flow.

Table 5. Thermal stability factor exhibited by individual mesogenic phases of PA + nBAO and PA + nBA series.

COMPLEX	N	G	COMPLEX	G
PA + 5BAO	—	1946	PA + 2BA	252
PA + 6BAO	—	1082	PA + 3BA	398
PA + 7BAO	—	213	PA + 4BA	330
PA + 8BAO	—	1393	PA + 5BA	166
PA + 9BAO	420	111	PA + 6BA	333
PA + 10BAO	1603	1446	PA + 7BA	350
PA + 11BAO	1290	789	PA + 8BA	116
PA + 12BAO	1554	644		

called stability factor (S). As a representative case the stability factor for smectic G, S_G, is given by

$$S_G = T_{\text{mid}} * \Delta T_G$$

T_{mid} is the mid smectic G temperature and ΔT_G, the smectic G thermal range. In this manner, the thermal stability of smectic G and nematic phase exhibited by different homologues are calculated and tabulated in Table 5 for both the PA + nBAO and PA + nBA homologous series. It can be noticed that the stability of smectic G phase is much reduced in PA + nBA series due to the absence of oxygen atom. Hence, the electronegative atom not only induces the mesogenic nature, but also enhances the phase stability, which proves the material to be fit for the applicational aspect.

Cox ratio

Navard and Cox [39] executed a new experimental method in determining the order of phase transition, where the scan rate of the sample or the weight of the sample can be a varying parameter with respect to the phase transition peak height obtained by DSC thermograms. In this present work, the variation is the scanning rate, viz., 5°C/min and10°C/min has been considered for practical convenience. According to Cox theory, the first- and second-order transitions can be classified basing on the ratio (Nc) of the measured phase transition peak heights. The ratio (Nc) is $1 < \text{Nc} \geq \sqrt{2}$ for an isothermal first-order transition and $\text{Nc} = 2$ for a second-order transition. Transition magnitudes exceeding $\sqrt{2}$ and nearing 2 can be considered as weak first-order transition. Table 6 illustrates the cox ratio of various mesophases corresponding to the PA + nBAO and PA + nBA homologous series.

Table 6. Phase transition order estimation.

Complex	Phase	Cox ratio	Order of transition	Complex	Phase	Cox ratio	Order of transition
PA + 5BAO	G	1.97	Second	PA + 2BA	G	1.0	First
PA + 6BAO	G	1.66	Weak first	PA + 3BA	G	0.25	First
PA + 7BAO	G	1.27	First	PA + 4BA	G	0.33	First
PA + 8BAO	G	1.57	Weak first	PA + 5BA	G	1.0	First
PA + 9BAO	N	2.34	Second	PA + 6BA	G	1.0	First
	G	0.01	First	PA + 7BA	G	1.5	Weak first
PA + 10BAO	N	0.33	First	PA + 8BA	G	2	Second
	G	1.42	First				
PA + 11BAO	N	1.64	Weak first				
	G	1.51	Weak first				
PA + 12BAO	N	1.44	First				
	G	1.40	First				

Influence of oxygen atom toward the mesomorphic properties

Presence/absence of the oxygen atom and its influence towards the mesomorphic properties exhibited by the designed thermotropic linear HBLC series (PA + nBAO and PA + nBA) are summarized.

(i) From the POM and DSC studies carried out (Tables 1 and 2), it is well noticed that the isotropic transition temperature, inducement of smectic G phase transition temperatures and crystalline temperatures are drastically reduced for the PA + nBA homologous series. Hence, absence of oxygen atom has influenced the phase transition temperatures to a greater extent.

(ii) Individual mesogenic phase range and the phase polymorphism is also modified, which is attributed to the above argument.

(iii) The length of the alkyl chain gets elongated with the presence of oxygen atom, which induces the flexibility of the complex. Thus, presence of electronegative oxygen atom (PA + nBAO) has initiated odd-even effect along phase transition temperatures and enthalpy values, which in missing in its counterpart (PA + nBA).

(iv) Magnitude of the total thermal equilibrium exhibited by the complexes almost possess same magnitude with an exception (PA + 8BAO and PA + 8BA) indicating the validity of thermal law (Table 4).

(v) Smectic G phase is observed to possess greater thermal stability in PA + nBAO series (Table 5) due to its wide thermal range. Presence of oxygen atom has favored in widening the thermal range of smectic G phase.

(vi) Order of phase transition is also affected by the oxygen atom for smectic G phase in both the homologous series even though the phase itself is a higher ordered phase.

Light filtering action

It is reported [40, 42] that nematic liquid crystal optical filters are capable of transmitting light substantially at all wavelengths while reflecting light over a single, generally narrow, wavelength band. From the literature of nematic liquid crystals [43], it can be inferred that the

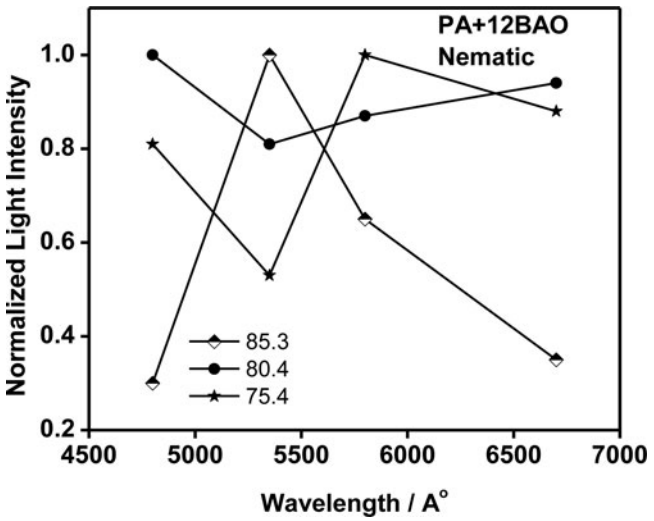

Figure 6a. Light Filtering action in PA + 12BAO complex.

unique optical properties of liquid crystal elements can be exploited to provide a wide variety of narrow band filtering functions extending over a wide wavelength range from the near ultraviolet to the far infrared. Figures 6a–6d represents the application of PA + nBAO complexes ($n = 12, 11, 10$, and 9) as different kinds of filters with respect to the desired wavelength. The normalization was done with respect to the maximum percentage of light transmitted from the nematogens.

From the observations made from Fig. 6a corresponding to PA + 12BAO homologue, the trend traced by the nematogens with temperature variation suggests the present complex to act as a notch filter and band pass filter at different temperatures. Similarly, Fig. 6b corresponding to PA + 11BAO complex indicates the complex to act as high pass and band pass filter by altering the temperature within the nematic thermal range. Figs. 6c and 6d relating to PA + 10BAO and PA + 9BAO clearly shows the utility of the complexes as notch filters.

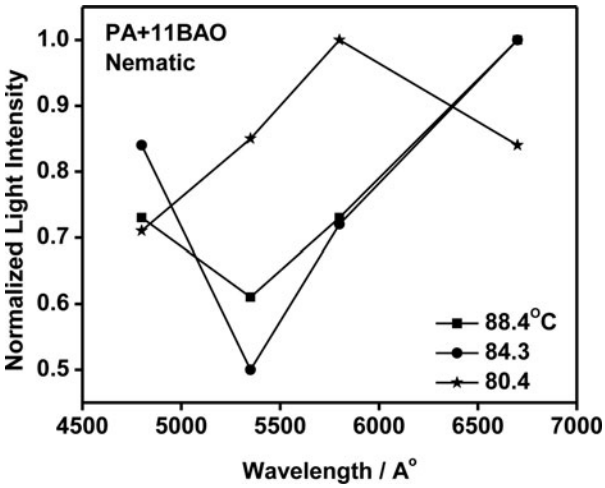

Figure 6b. Light Filtering action in PA + 11BAO complex.

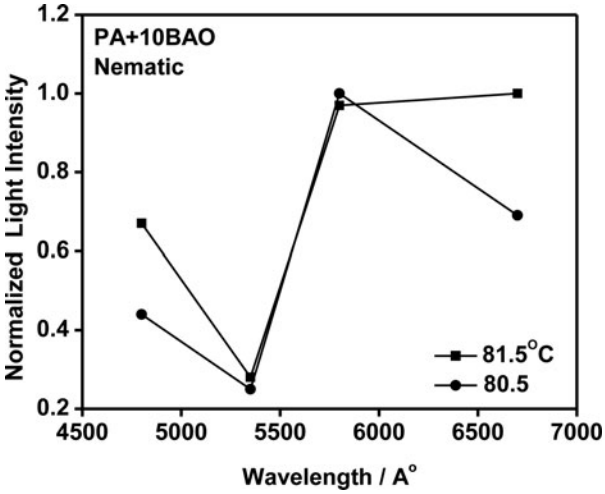

Figure 6c. Light Filtering action in PA + 10BAO complex.

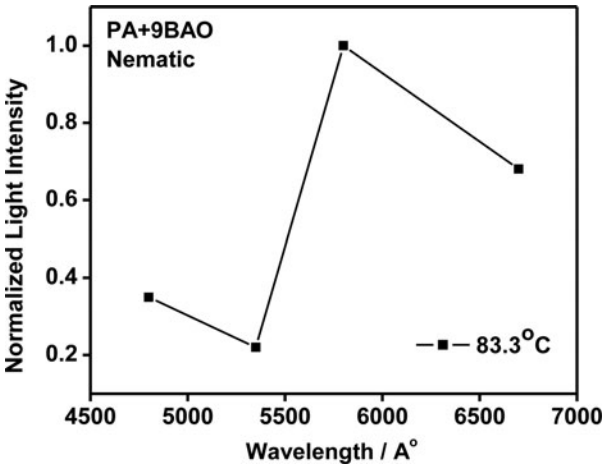

Figure 6d. Light Filtering action in PA + 9BAO complex.

Conclusions

(i) Two novel series of linear hydrogen-bonded thermotropic liquid crystals are designed and characterized by various techniques.
(ii) Influence of electronegative oxygen atom attached or detached to the rigid part of the chemical moiety is elaborated.
(iii) Thermal span of the mesogenic phase, their thermal stability factor, corresponding order of transition are also compared between the designed homologous series (PA + nBAO and PA + nBA).
(iv) Application of nematogens as desired filters is carried out.

Acknowledgments

Eternal blessings showered by Almighty Bannari Amman and infrastructural support provided by Bannari Amman Institute of Technology are gratefully acknowledged.

References

[1] Quan, Li. (2012). *Liquid Crystals Beyond Displays*, Wiley: New Jersey.
[2] Goodby, J. W. (2011). *Liq. Cryst.*, *38*, 1363.
[3] Deng Ke, Y., & Shin–Tson, Wu. (2015). *Fundamentals of Liquid Crystal Devices*, Wiley: United Kingdom.
[4] Pochi, Y., & Claire, Gu. (2010). *Optics of Liquid Crystal Displays*, Wiley: New Jersey.
[5] Paleos, C. M., & Tsiourvas, D. (1995). *Angew. Chem. Int. Ed. Engl.*, *34*, 1696.
[6] Gray, G. W. (1967). *Molecular Structure and Liquid Crystals*, Academic Press: London.
[7] Kelker, H., & Hatz, R. (1980). *Hand Book of Liquid Crystals*, Verlag Chemie: Weinheim.
[8] Vorliinder, D. (1908). *Ber. Dtsch. Chem. Ges.*, *41*, 2033.
[9] Gray, G. W., & Jones, B. (1954). *J. Chem. Soc.*, 1467.
[10] Gray, G. W., & Jones, B. (1953). *J. Chem. Soc.*, 4179.
[11] Pongali Sathya Prabu, N., & Madhu Mohan, M. L. N. (2012). *Phase Transitions.*, *85*, 592.
[12] Pongali Sathya Prabu, N., & Madhu Mohan, M. L. N. (2012). *Mol. Cryst. Liq. Cryst.*, *557*, 190.
[13] Pongali Sathya Prabu, N., & Madhu Mohan, M. L. N. (2012). *Mol. Cryst. Liq. Cryst.*, *562*, 177.
[14] Pongali Sathya Prabu, N., & Madhu Mohan, M. L. N. (2012). *Mol. Cryst. Liq. Cryst.*, *569*, 72.

[15] Kavitha, C., Pongali Sathya Prabu, N., & Madhu Mohan, M. L. N. (2013). *Mol. Cryst. Liq. Cryst.*, *574*, 96.
[16] Gopunath, A. J., Chitravel, T., Kavitha, C., Pongali Sathya Prabu, N., & Madhu Mohan, M. L. N. (2013). *Mol. Cryst. Liq. Cryst.*, *574*, 19.
[17] Gopunath, A. J., Chitravel, T., Kavitha, C., Pongali Sathya Prabu, N., & Madhu Mohan, M. L. N. (2014). *Mol. Cryst. Liq. Cryst.*, *592*, 1.
[18] Rajanandkumar, R., Pongali Sathya Prabu, N., & Madhu Mohan, M. L. N. (2013). *Mol. Cryst. Liq. Cryst.*, *587*, 60.
[19] Hariharan, V., Pongali Sathya Prabu, N., & Madhu Mohan, M. L. N. (2014). *Mol. Cryst. Liq. Cryst.*, *594*, 1.
[20] Sangameswari, G., Pongali Sathya Prabu, N., & Madhu Mohan, M. L. N. (2015). *Phase Tranitions.*, *88*, 907.
[21] Paleos, C. M., & Tsiourvas, D. (2001). *Liq. Cryst.*, *28*, 1127.
[22] Sherrington, D. C., & Taskinena, K. A. (2001). *Chem. Soc. Rev.*, *30*, 83.
[23] Lehn, J. M. (1995). *Supramolecular Chemistry*, Wiley-VCH: Weinheim, New York.
[24] Philippe, M., Marianne, C., Michele, V., & Robert, D. (2005). *Chem. Mater.*, *17*, 1946.
[25] Fouquey, C., Lehn, J. M., & Mlevelut, A. (1990). *Adv. Mater.*, *2*, 254.
[26] Gray, G. W., & Good by, J. W. G. (1984). *Smectic Liquid Crystals: Textures and Structures*, Leonard Hill: London.
[27] Kato, T., Uryu, T., Kaneuchi, F., Jin, C., & Frechet, J. M. J. (1993). *Liq. Cryst.*, *14*, 1311.
[28] Pavia, D. L., Lampman, G. M., & Kriz, G. S. (2007). *Introduction to Spectroscopy*, Sanat Printers: India.
[29] Nakamoto, K. (1978). *Infrared and Raman Spectra of Inorganic and Co-ordination Compounds*, Interscience: New York.
[30] Xu, J. (2006). *J. Mater. Chem.*, *16*, 3540.
[31] Frechet, J. M. J., & Kato, T., in US Patent, Number 5,139,696, dt.Aug18, 1992.
[32] Marcelja, S. (1973). *Solid State Commun.*, *13*, 759.
[33] Chandrasekhar, S. (1977). *Liquid Crystals*, Cambridge University Press: New York.
[34] Thoen, J., Cordoyiannis, G., & Glorieux, C. (2009). *Liq Cryst.*, *36*, 66.
[35] Marcelja, S. (1974). *J. Chem. Phys.*, *60*, 3599.
[36] Senthil, S., Rameshbabu, K., & Wu, S. L. (2006). *J. Mol. Struct. 783*, 215.
[37] Smith, G. W., & Gardlund, Z. G. (1973). *J. Chem. Phys.*, *59*, 3214.
[38] Osman, Z. (1976). *Z. Naturforsch.*, *31b*, 801.
[39] Navard, P., & Cox, R. (1984). *Mol. Cryst. Liq. Cryst.*, *102*, 261.
[40] Adams, J. E. (1972). U.S. Pat. No. 3,679,290.
[41] Adams, J. E. (1973). U.S. Pat. No. 3,711,181.
[42] Pongali Sathya Prabu, N. (2014). *Physico-Chemical Investigations in Self-Assembled Hydrogen Bonded Liquid Crystals*, Anna University: Chennai.
[43] Goldberg, P., Hansford, J., & Van Heerden, P. J. (1971). *J. Appl. Phys., 42*(10), 3874.